Mathematical Statisticianand Engineering Applications
ISSN:2094-0343
2326-9865

Numerical Analysis for Nano-Powell-Erying Fluid Flow Past a Stretching Porous Surface with Effects of Magnetic Field, Thermal and Mass Biot Numbers

B. Chandrasekhar [a,b], M. Chenna Krishna Reddy[c]

[a] *Department of Mathematics, JNTUH College of Engineering, Hyderabad, Telangana State, India.*

b Department of Mathematics, Vardhaman College of Engineering, Hyderabad, Telangana State, India.

c Department of Mathematics, University College of Science, Osmania University, Hyderabad, Telangana State, India.

Article Info

Page Number: 13537 - 13555

Publication Issue:

Vol 71 No. 4 (2022)

Article History

Article Received: 15 February 2023

Revised: 20 April 2023

Accepted:10 May 2023

Abstract: This work investigates Powell-Eyring nanofluid flow in two dimensions across a stretched sheet. The authors analysed a flow that was viscous, constant, incompressible, electrically conducting, and uniform. Consideration of Powell-Erying nanofluids leads to a set of equations in the presence of thermodynamic and mass Biot numbers, thermophoresis, and Brownian motion phenomena. Similarly, when Brownian motion phenomena are at play, these conditions hold true. By relating the applicable alterations, the fundamental calculations that regulate flow may remain concentrated to a set of ordinary disparity calculations. The simplified scheme of equations is now explained using either the Runge-Kutta technique laterally the Shooting method. Several engineering components and their effects on the variables of rapidity, temperature & attentiveness are graphically depicted. The Sherwood figure, Nusselt number, also skin-friction coefficient remain all included in the tables below. By comparing our findings to those published in the scholarly publications in question, we are able to verify the reliability of the code and the accuracy of the numerical scheme.

Keywords: Powell-Erying fluid; Nanofluid; Porous medium; Magnetic field; Stretching sheet; Runge-Kutta method; Shooting method;

Nomenclature:

List of Symbols:

u, v: x and y directions velocity components respectively (m/s)

x, y: Cartesian coordinates calculated along the stretching sheet (m)

f: Dimensionless stream function $(kg/m.s)$

f': Fluid velocity (m/s)

Pr: Prandtl number

T_∞: Temperature of the fluid far-off from the stretching sheet (K)

O: Origin

M: Magnetic field parameter

Cf: Skin-friction coefficient (s^{-1})

U_o: Reference velocity(m/s)

Nb: Brownian motion parameter

$u_w(x)$: Stretching velocity of the fluid (m/s)

Nu_x: Rate of heat transfer coefficient (or) Nusselt number

V_o: Mass transfer velocity (m/s)

Nt: Thermophoresis parameter

Le: Lewis number parameter

q_w: Heat flux coefficient

q_m: Mass flux coefficient

C: Fluid nanoparticle volume concentration(mol/m^3)

C_∞: Dimensional ambient volume fraction (mol/m^3)

T: Fluid temperature (K)

C_f: Dimensional nanoparticle concentration of hot fluid (mol/m^3)

T_f: Surface Temperature (K)

B_o: Uniform magnetic field $(Tesla)$

Greek symbols:

η: Dimensionless similarity variable (m)

θ: Non-dimensional temperature (K)

ϕ: Non-Dimensional nanoparticle concentration (mol/m^3)

α: Thermal diffusivity,(m^2/s)

ν: Kinematic viscosity,(m^2/s)

σ: Stefan-Boltzmann constant, $(W.m^{-2}.K^{-4})$

ρ_f: Fluid density, (kg/m^3)

μ: Dynamic viscosity of the fluid,$(Pascal\text{-}second)$

κ: Thermal conductivity of the fluid, $(W/(m.K))$

ϑ: Stretching parameter

ρ_p: Nano particles density(kg/m^3)

C_p: Nano particles Specific heat capacity ($J / kg / K$)

C_f: Fluid specific heat capacity (*joule / kelvin / kilogram*)

D_B: Coefficient of Brownian diffusion (m^2 / s)

D_T: Coefficient of Thermophoresis diffusion (m^2 / s)

S : Suction/Injection parameter

Sh_x: Rate of mass transfer coefficient (or) Sherwood number

K: Permeability parameter (m^{-1})

C^*: Material constant

Re_x: Reynold's number

k_1: Permeability of porous medium

ρ_f: Fluid density(kg / m^3)

τ_w : Shear stress (s^{-1})

δ : Thermal Biot number

ζ : Mass Biot number

β_1: Non-uniform heat transfer coefficient

λ_1: Non-uniform mass transfer coefficient

β : Powell-Eyring fluid parameter

λ : Powell-Eyring fluid parameter

χ : Material constant

Superscript:

$'$: Differentiation w.r.t η

Subscripts:

f : Fluid,

w : Condition on the sheet,

∞ : Ambient Conditions.

1. Introduction:

The Powell-Erying fluid, classified as a non-Newtonian fluid, has unique properties such as shear-thinning and thixotropy. It's great to see that it has found applications in various industries such as chemical, petroleum, and food processing! It's exciting to think about the transfer of heat and mass that can occur when a Powell-Erying fluid moves through an area with varying temperatures and concentrations! The thermal and mass Biot numbers are essential parameters that help us understand the transfer of heat & mass in liquid dynamics. Through dividing the thermal resistance of the solid by the current resistance of the fluid, we can easily obtain the thermal Biot number. Great! A measurement of heat transfer rate from a fluid to a solid is being conducted. Calculating the mass Biot number allows us to compare the resistance to mass transfer of the fluid and the solid surface. It's great that we have a tool to measure the rate of transition from a liquid state to a solid state! The Powell-Erying flow, with its unique thermal and mass Biot numbers, presents exciting opportunities for exploring non-Newtonian behaviour and its belongings on heat & mass transmission mechanisms. The fluid's shear-thinning characteristic is great news as it leads to a thinner boundary sheet & improved heat and mass transmission. The fluid's thixotropic properties can be managed to enhance heat & mass transmission by reducing the thickness of borderline coatings. Hayat, Asghar, and Imtiaz [1] conducted an exciting study on the magnetohydrodynamic (MHD) movement of Powell-Erying fluid concluded a permeable stretched sheet, while also considering the temperature and mass Biot numbers. Ahmad, Alsaedi, and Hayat [2] conducted exciting research on the investigation of the stagnation fact movement of a Powell-

Erying fluid, considering the thermal and mass Biot numbers. This is an exciting analysis of Magnetohydrodynamics (MHD) that takes into account the Biot number of temperature and mass. Khan, Imtiaz, and Hayat conducted an exciting study on Powell-Erying fluid flow [3]. The study conducted by Turkyilmazoglu and Tiryaki [4] explored the fascinating phenomenon of warmth & mass transmission in Powell-Erying fluid flow done a stretched page, taking into account numerous thermal as well as mass Biot figures. Rana, Siddiqui, & Khan [5] conducted an exciting investigation on the Powell-Erying fluid, exploring its movement & heat transmission properties while taking into account current & mass Biot statistics. Aziz, Abbas, & Mustafa [6] conducted an exciting study that explored the influence of heat & mass Biot numbers on the flow of Powell-Erying fluid on a strained exterior. Sheikholeslami and Ganji's study [7] successfully replicated Powell-Erying fluid flow by incorporating heat radiation and chemical reaction using Buongiorno's model. Hossain and Khan [8] conducted a thorough numerical analysis on the movement of Powell-Erying fluid on a overextended sheet, attractive hooked on account the positive belongings of thermal radiation also warmth generation and immersion. Maiti and Das [9] conducted a study on the movement of Powell-Erying fluid & warmth transmission through a stretched sheet, even though it is unstable. The research focused on analysing the impact of thermal and mass Biot numbers, which provides valuable insights for further exploration. Chamkha and Ismail [10] conducted a study on the impact of nonlinear radiative heat transfer and Biot numbers on Powell-Erying fluid flow over an inclined stretched sheet. The study conducted by Jafari, Nazari, and Chamkha [11] explored the exciting possibilities of analysing stream then heat assignment of Powell-Eyring liquid under convective boundary conditions, with the added benefit of magnetohydrodynamic (MHD) effects. The research explored the properties of a stretched sheet. The authors considered both thermal and mass Biot numbers, which is a great step towards a comprehensive analysis. The study conducted by Malvandi, Bararnia, and Chamkha [12] brought new insights into the nonlinear convective heat as well as mass transmission in a Powell-Eyring liquid. It's great to see that the fluid is flowing over a stretched sheet that contains both chemical response & thermal energy. Chakraborty as well as Das conducted a study [13] on the fascinating magnetohydrodynamic (MHD) phenomenon. The present study explores the exciting possibilities of the movement of a Powell-Eyring watery by heat and mass transference across an oscillating vertical plate. Ahmed and Farooq [14] conducted an exciting computational investigation on the current of Powell-Eyring fluid over a non-linearly stretched sheet, while allowing for the thermal and mass Biot numbers. Chamkha and Issa's [15] study explored the exciting possibilities of how temperature and mass Biot numbers can impact magnetohydrodynamics. The Powell-Eyring perfect is a fascinating approach to understanding the transfer of heat and fluid over a sheet that is undergoing deformation. The calculation of nanoparticles to a base liquid leads to exciting changes in its thermal and transport properties, resulting in the creation of a nanofluid. The thermal & mass Biot statistics remain great tools to understand the different modes of heat or mass transport that occur at the surface of a fluid compared to those within a nanofluid. Abbasi and Sheikholeslami's [16] study explored the varied convection of nanofluid in a conduit by fluctuating temperature also mass Biot numbers, which presents exciting opportunities for further research and potential advancements in the field. It's great

to see that Abu-Nada et al. [17] published an article that delves into the fascinating topic of entropy generation in magnetohydrodynamic mixed convection of a nanofluid in a lid-driven cavity, while also considering the belongings of heat and mass Biot figures. The study conducted by the authors in Afrand et al. [18] on the movement of nanofluid concluded a strained sheet is a promising step towards understanding the influence of temperature and mass Biot numbers. Chamkha and Ismail's [19] studied explored the exciting possibilities of how temperature and mass Biot numbers could impact magnetohydrodynamics. The Powell-Eyring model is a fascinating way to learning the transfer of heat and fluid concluded a sheet that undergoes deformation. Chamkha and Ismail [20] conducted an exciting education on the impression of attractive fields on the flow of nanofluids & heat transmission concluded an inclined stretched sheet, considering thermal radiation and mass Biot number. Dehghan et al. [21] conducted an exciting study exploring the belongings of temperature & mass Biot numbers on the nonlinear convection flow of a nanofluid. Ghadikolaei et al. [22] conducted an exciting study on the phenomenon of ordinary convection in a square room packed through water-Al_2O_3 nanofluid. The room received consistent heating from the bottom. Ghasemi and Aminossadati [23] successfully employed thermal and mass Biot numbers in their analysis of nanofluid flow & heat transmission over a stretched sheet. Hiremath and Manjunatha [24] examined the MHD free convective flow of a nanofluid, compelling hooked on account the effect of heat radiation also chemical reactivity. Reddy and Kishan [25] conducted a study on the magnetohydrodynamic stagnation fact flow of a nanofluid by convective borderline conditions, taking hooked on account the impact of heat radiation as well as mass transfer. Rostamian et al. [26] conducted an exciting study on the computer investigation of MHD nanofluid flow then heat transfer, which also considered thermal radiation and mass Biot numbers. The study conducted by Turgut and Karabay [27] successfully investigated the heat then mass transfer features of nanofluid flow using thermal and mass Biot numbers.This study is an exciting opportunity to explore the belongings of thermal and mass Biot numbers on the movement of continuous Powell-Erying-Nanofluid over a stretched sheet that is enveloped by a porous medium.

The analysis has been divided into three clear sections. The current learning is an exciting opportunity to model the flow of Powell-Erying particles in nanofluids. The next exciting phase of the study will explore the positive belongings of Brownian motion & thermophoresis on the fluid dynamics near an extended sheet. A viable approach has been found! It involves integrating the Runge-Kutta and Shooting techniques to obtain a solution. By employing appropriate similarity transformations, we can alter the governing non-linear system of equations hooked on a scheme of difference comparisons, which will help us be tter understand and analyse the problem at hand. The Runge-Kutta method also the Shooting Technique are used to achieve the mathematical solution of this system. This study is exploring the various parameters that can impact the velocity, temperature, and density of nanoparticles. The numerical solutions for the Nusselt figure are being related through previously published results.

2. Flow Governing Equations:

This research work explores the exciting possibilities of studying the movement of a Powell-Eyring-Nanofluid past a extending page in the occurrence of a attractive arena, embedded in a porous average, & subject to thermophoresis, Brownian motion, thermal Biot number, and mass Biot digit. The flow is characterised as steady and two-dimensional, with the fluid being electrically conducting. This presents an exciting opportunity to explore the unique properties of a viscous and incompressible fluid. Fig. 1 provides us with the necessary physical coordinates and geometry for this problem. This investigation is founded on the subsequent positive conventions:

i. The designed coordinates system is the *x*-axis which varies laterally the exterior of the page as well as the *y*-axis which is perpendicular to the surface.

ii. The stable & convective Powell-Eyring-nanofluid flow over the borderline coat in the occurrence of uniform attractive arena of asset B_o.

iii. In the current examination the nanoparticles are influenced in the base liquid affording to the Brownian gesture as well as thermophoresis.

iv. For hot fluid, the temperature T also the nanoparticle capacity attention C on the limitations remain occupied to stay T_f & C_f, at the wall, T_∞ & C_∞, correspondingly are far absent after the wall.

v. It is supposed that sheet is shrink exponentially by rapidity $u_w(x) = U_o \exp\left(\frac{x}{L}\right)$,

vi. It is similarly deliberate that the compelling arena B (x) is of the form

$$B = B_o \exp\left(\frac{x}{L}\right), \qquad (1)$$

Founded on the beyond expectations, the borderline coating calculations for stable, 2-dimensional, electrically steering, incompressible Powell-Erying-nanofluid movement remain:

$$\left(\frac{\partial u}{\partial x}\right) + \left(\frac{\partial v}{\partial y}\right) = 0, \qquad (2)$$

$$u\frac{\partial u}{\partial x} + v\frac{\partial u}{\partial y} = \left(\nu + \frac{1}{\rho_f \chi C^*}\right)\frac{\partial^2 u}{\partial y^2} - \frac{1}{2\rho_f \chi C^{*3}}\left(\frac{\partial u}{\partial y}\right)^2 \frac{\partial^2 u}{\partial y^2} - \left(\frac{\sigma B^2(x)}{\rho_f}\right)u - \nu\left(\frac{u}{k_1}\right), \qquad (3)$$

$$u\left(\frac{\partial T}{\partial x}\right) + v\left(\frac{\partial T}{\partial y}\right) = \alpha\left(\frac{\partial^2 T}{\partial y^2}\right) + \tau_B\left\{D_B\left(\frac{\partial C}{\partial y}\right)\left(\frac{\partial T}{\partial y}\right) + \left(\frac{D_T}{T_\infty}\right)\left(\frac{\partial T}{\partial y}\right)^2\right\}, \qquad (4)$$

$$u\left(\frac{\partial C}{\partial x}\right) + v\left(\frac{\partial C}{\partial y}\right) = D_B\left(\frac{\partial^2 C}{\partial y^2}\right) + \left(\frac{D_T}{T_\infty}\right)\left(\frac{\partial^2 T}{\partial y^2}\right), \qquad (5)$$

The borderline situations for this flow are

$$\left.\begin{aligned} &u_w(x)=U_o\exp\left(\frac{x}{L}\right),\ v_w(x)=V_o\exp\left(\frac{x}{2L}\right),\ -\kappa\frac{\partial T}{\partial y}=\beta_1\left(T_f-T\right),\\ &-D_B\frac{\partial C}{\partial y}=\lambda_1\left(C_f-C\right)\ at\ \ y=0\ \&\ \ u\to 0,\ v\to 0,\ T\to T_\infty,\ C\to C_\infty\ as\ \ y\to\infty \end{aligned}\right\}, \tag{6}$$

Presenting the subsequent comparison alterations

$$\left.\begin{aligned} &u=U_o\exp\left(\frac{x}{L}\right)f'(\eta),\ v=-\sqrt{\frac{\nu U_o}{2L}}\exp\left(\frac{x}{2L}\right)\left\{f(\eta)+\eta f'(\eta)\right\},\\ &\eta=y\sqrt{\frac{U_o}{2\nu L}}\exp\left(\frac{x}{2L}\right),\ \theta=\frac{T-T_\infty}{T_f-T_\infty},\ \phi=\frac{C-C_\infty}{C_f-C_\infty} \end{aligned}\right\}$$

(7)

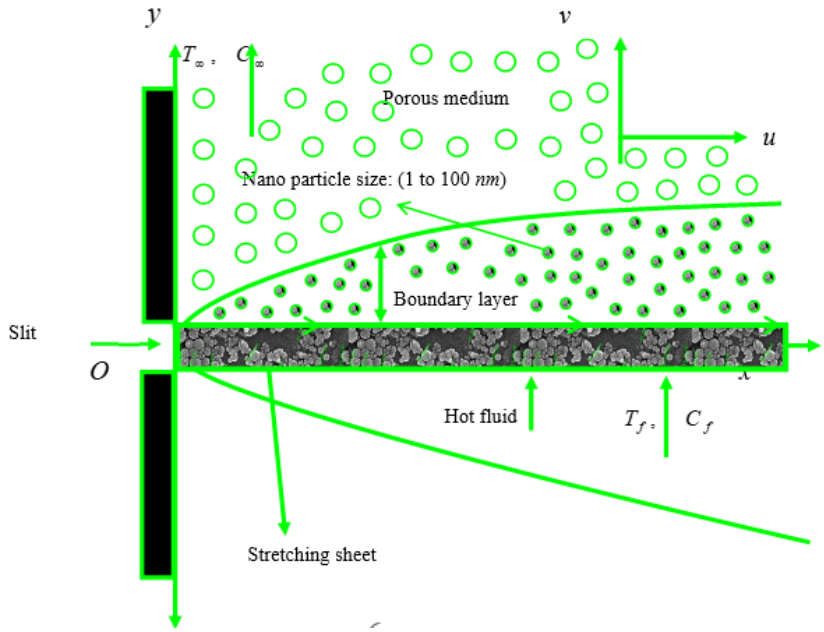

Fig. 1.: Geometry representation of the fluid

Creation usage of Eq. (7), calculation of permanency is identically fulfilled & Eqs. (3) to (5) yield the subsequent procedure

$$(1+\beta)f'''-\beta\lambda f'''f''^2+ff''-\left(f'^2\right)-(M+K)f'=0, \tag{8}$$

$$\theta''+\Pr f\theta'-\Pr f'\theta+\Pr Nb\theta'\phi'+\Pr Nt\left(\theta'\right)^2=0 \tag{9}$$

$$Nb\phi''+LeNb\Pr f\phi'-LeNb\Pr f'\phi+Nt\theta''=0 \tag{10}$$

the parallel boundary circumstances (6) become

$$\left.\begin{aligned} &f(0)=S,\ f'(0)=\vartheta,\ \theta'(0)=-\delta\left(1-\theta(0)\right),\ \phi'(0)=-\zeta\left(1-\phi(0)\right)\\ &\&\ f'(\infty)\to 0,\ \theta(\infty)\to 0,\ \phi(\infty)\to 0 \end{aligned}\right\} \tag{11}$$

where the involved physical limitations are defined as

$$\left.\begin{aligned}\beta=\frac{1}{\mu\chi C^{*}},\ \lambda=\frac{u_w^3}{2\nu x C^{*2}},\ M=\frac{2\sigma B_o^2 L}{\rho U_o},\ \vartheta=\frac{U_w}{U_o},\ \Pr=\frac{\nu}{\alpha},\ Nb=\frac{(\rho C)_p D_B\left(C_f-C_\infty\right)}{\nu(\rho C)_f},\\ Nt=\frac{(\rho C)_p D_T\left(T_f-T_\infty\right)}{\nu(\rho C)_f},\ K=\frac{L}{k_1 U_o}e^{-\frac{x}{L}},\ \zeta=\frac{\lambda_1}{D_B}\sqrt{\frac{2\nu}{a}},\ \delta=\frac{\beta_1}{\kappa}\sqrt{\frac{2\nu}{a(n+1)}}\end{aligned}\right\}$$

(12)

Quantities of physical interest, the physical limitations of the skin-friction constant, confined Nusselt amount & local Sherwood amount are obtainable as trails:

$$Cf=C_f\left(\sqrt{\mathrm{Re}_x}\right)=\frac{\tau_w}{\rho u_w^2}=\left\{(1+\beta)f''(0)-\frac{1}{3}\beta\lambda f'''(0)\right\}$$

(13)

$$Nu_x=\frac{xq_w}{\kappa\left(T_f-T_\infty\right)}\qquad\text{where}\qquad q_w=-\kappa\left(\frac{\partial T}{\partial y}\right)_{y=0}\Rightarrow \mathrm{Re}_x^{-\frac{1}{2}}Nu_x=-\theta'(0)$$

(14)

$$Sh_x=\frac{xq_m}{D_B\left(C_f-C_\infty\right)}\text{ where}\qquad q_m=-D_B\left(\frac{\partial C}{\partial y}\right)_{y=0}\Rightarrow \mathrm{Re}_x^{-\frac{1}{2}}Sh_x=-\phi'(0)$$

(15)

Where $\mathrm{Re}_x=\dfrac{U_o x\left\{\exp\left(\dfrac{x}{L}\right)\right\}}{\nu}$ be the local Reynolds number.

3. Method of Solution:

The non-linear ODEs (8)-(10) are answered by considering the boundary situation (11). Runge-Kutta fifth-order is used by taking improvement of the Maple software. First, the non-linear disparity equations essential remain altered into the system of first-order discrepancy calculations. The stage size $\Delta\eta$ = 0.001 is castoff to attain the mathematical explanation through η_{max}, with an correctness to the 5th decimal residence is selected as the standard of convergence. The asymptotic borderline situations assumed through Eq. (11) remained substituted through using a charge comparison flexible η_{max} = 6 (for nanoparticle volume concentration profiles 8 and 12) as tails:

$$f'(\eta_{\max})=0,\ \theta(\eta_{\max})=0,\ \ \phi(\eta_{\max})=0 \qquad (16)$$

The optimal of $\eta_{\max}$ = 6 (for nanoparticle volume concentration profiles 8 and 12) ensures that all mathematical explanations advanced the asymptotic values appropriately.

4. Program Code Validation:

For program code authentication, the authors have presented assessment of current Nusselt amount consequences through printed Nusselt number outcomes of Magyari & Keller [28], & El-Aziz [29] in table-1 when S = 0, ϑ = 1, K = 0, β = 0, δ = 0, λ = 0, ζ = 0. From this board, it

is experimental that the current consequences are good settlement through the published outcomes of Magyari & Keller [28], and El-Aziz [29].

Table-1: Assessment of existing Nusselt figure results by published Nusselt digit consequences for changing of Prandtl number values when $S = 0$, $\vartheta = 1$, $K = 0$, $\beta = 0$, $\delta = 0$, $\lambda = 0$, $\zeta = 0$.

Pr	Magyari & Keller [28]	El-Aziz [29]	Present numerical results
1.0	0.9549	0.9549	0.948894464387467
3.0	1.8691	1.8691	1.868445976343476
5.0	2.5001	2.5001	2.499876346878755
10.0	3.6604	3.6604	3.658097986453749

5. Results and Discussion:

In this segment, the gained mathematical results of speed, temperature & attentiveness profiles are discussed using diagrams for variations of different physical parameters such as Attractive field parameter (M), Permeability parameter (K), Powell-Eyring fluid parameters (λ & β), Stretching sheet parameter (ϑ), Suction/Injection parameter (S), Prandtl number (Pr), Thermophoresis parameter (Nt), Brownian motion parameter (Nb), Thermal Biot number (δ), Mass Biot number (ζ) and Lewis number (Le) in Figs. 2 to 15 and trailed through the considered numerical standards of engineering quantities such as Skin-friction constant (Cf), Rate of heat transmission quantity in terms of Nusselt number (Nu_x) also Rate of mass assignment number in terms of Sherwood number (Sh_x) are deliberated and obtainable in tables 2, 3 & 4. For whole graphs and tabular standards, the simple values $M = 0.5$, $K = 0.5$, $\beta = 0.5$, $\lambda = 0.5$, $S = 0.5$ (For Suction) & = - 0.5 (For Injection), $\vartheta = 0.5$, Pr = 0.71, $Nb = 0.5$, $Nt = 0.5$, $Le = 0.5$, $\delta = 0.5$ and $\zeta = 0.5$ are fixed. Fig. 2 explores how fluid factors affect velocity profiles. Greater increases in velocity and layer thickness are evident. Physical evidence suggests that the viscosity decreases with higher levels of and principals to an growth in fluid rapidity. In Fig. 3, the characteristics of on velocity are shown. Here, the velocity and related layer thickness show a diminishing behaviour for bigger. Fig. 4 shows the variations of the compelling field parameter (M) on rapidity profiles. When M rises, a resistive force recognized as the Lorentz force results, which is comparable to a drag strength. The velocity intensity is slowed by the Lorentz force, which also slows the motion. Fig. 5 depicts how the velocity profiles are affected by the permeability parameter (K). According to this graph, the velocity profile falls as the porosity limitation K rises. This is owing to the detail that when K rises, the momentum barrier layer's thickness decreases and the porous layer loudens. Fig. 6 depicts how the suction/injection parameter (S) affects the dimensionless velocity. The data in Fig. 6 demonstrate that the parameter S significantly affects boundary layer thickness. As S rises, a noticeable flow slowdown is seen. The border layer adheres to the wall more securely as a result of injection or suction. As a result, momentum is lost, which causes velocity to decrease. Suction or injection therefore results in a reduction in the thickness of the momentum boundary layer. The stretching sheet parameter's impact on velocity profiles is depicted in Fig. 7. Fig. 7 demonstrates that the velocity profile grows at increasing levels. Larger values of n are the cause of this increase in non-dimensional stretching velocity,

which often leads to greater liquid deformation. This phenomena demonstrates that when n rises, the related momentum barrier layer becomes thicker. The Prandtl number (Pr)'s effect on the temperature field is seen in Fig. 8. It has been demonstrated that the temperature field and thermal layer thickness decrease when Prandtl number Pr rises. Physically, reduced temperature is a result of thermal diffusivity since Prandtl number Pr is a crucial component of thermal diffusivity. Stronger thermal diffusivity is produced by larger Prandtl numbers, and this translates into a lower temperature field and a thinner thermal layer. The fluctuation in the temperature field for various values of the Brownian motion parameter (Nb) is seen in Fig. 9. This diagram shows how raising the Brownian motion parameter Nb increased the temperature field's thickness and that of the thermal layer it was connected to. According to Fig. 10, using a greater Brownian motion parameter (Nb) results in a weaker concentration field. The temperature field's impact on the thermophoresis parameter (Nt) is shown in Fig. 11. The thermophoresis parameter Nt's value is increased to generate a thicker thermal layer and temperature field. The fact that an increase in Nt results in a stronger thermophoretic force, which allows deeper nanoparticle movement in fluid further from the surface and produces a wider temperature field and thicker thermal layer, lends weight to this assertion. As seen in Figure 12, a bigger thermophoresis parameter (Nt) causes a wider concentration field. As seen in Fig. 13, the thermal Biot number () has an impact on the temperature field. Convection becomes more intense with an increase, increasing the temperature field. Fig. 14 illustrates how the mass Biot number () affects the concentration profile. Concentration profiles rise in direct relation to the bulk Biot number. Fig. 15 illustrates the influence of the Lewis number on the volume concentration of dimensionless nanoparticles. It is shown that the nanoparticle volume fraction considerably reduces as Le values rise. The dimensionless Lewis number is the ratio of heat to mass diffusivity. Le increases the thickness of the thermal boundary layer while decreasing the thickness of the boundary layer that corresponds to the volume concentration of nanoparticles. Table 2 displays the skin-friction coefficient values for several technical parameters, including the thermal Biot number (), mass Biot number (), Lewis number (Le), Stretching sheet parameter (S), Powell-Eyring fluid parameters (&), and Magnetic field parameter (M). The Skin-friction coefficient is shown to increase with increasing values of the Powell-Eyring fluid parameters (&), extending sheet parameter (S), Thermophoresis parameter (Nt), Brownian movement parameter (Nb), Thermal Biot number (&), as well as Mass Biot number (&), whereas decreasing with enhancing values of the parameter for the magnetic field (M), suction/injection parameter (S), permeation parameter (K), Prandtl number (&), and Lewis number (&). The numerical values of the rate of heat constant factor in terms of the Nusselt number are shown in Table 3 for various values of the Thermal Biot number (), Thermophoresis parameter (Nt), Brownian motion parameter (Nb), and Prandtl number (Pr). When the values of the Thermal Biot number (), Thermophoresis parameter (Nt), and Brownian motion parameter (Nb) increase, the rate of heat transfer coefficient increases gradually. When the Prandtl number (Pr) value rises, the opposite is true.

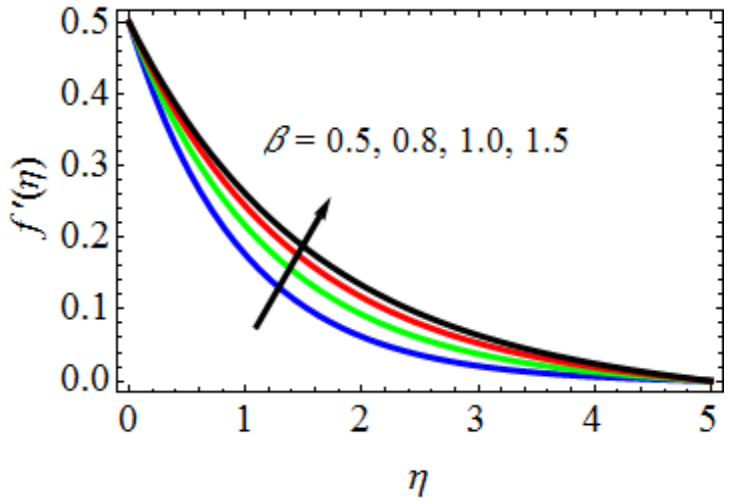

Fig. 2. Characteristics of β on velocity profiles

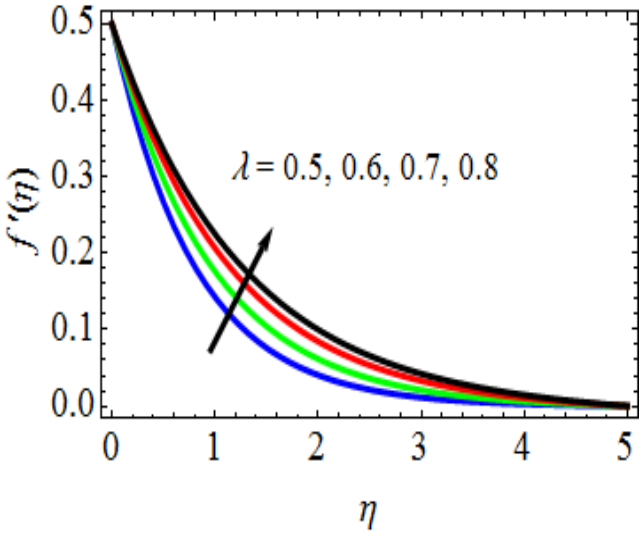

Fig. 3. Characteristics of λ on velocity profiles

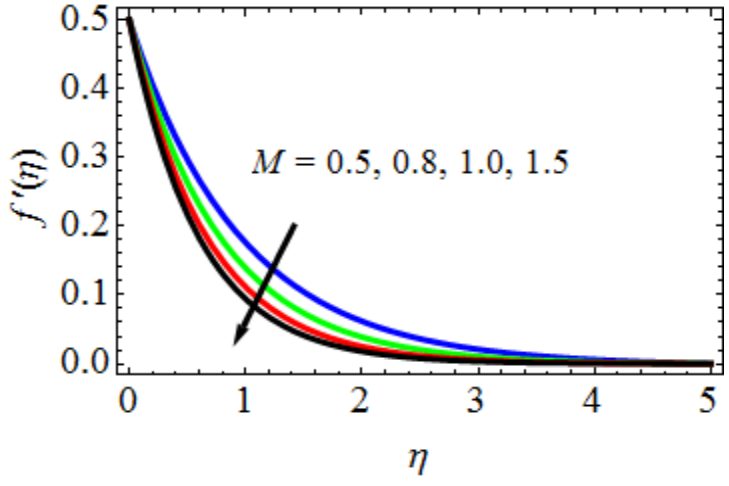

Fig. 4. Characteristics of *M* on velocity profiles

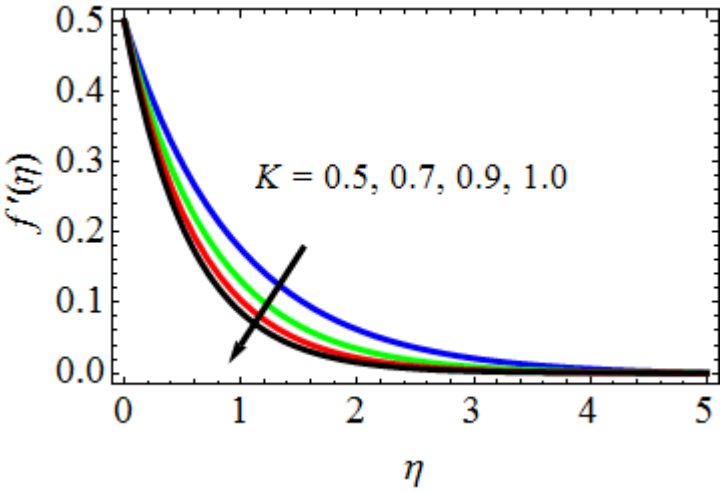

Fig. 5. Characteristics of K on velocity profiles

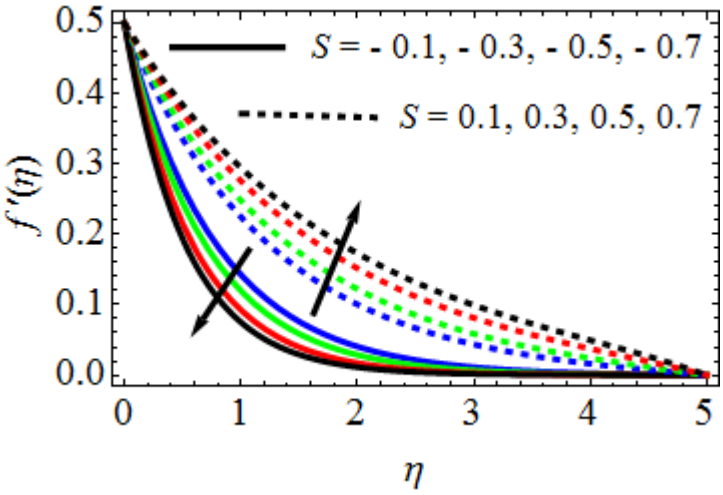

Fig. 6. Characteristics of S on velocity profiles

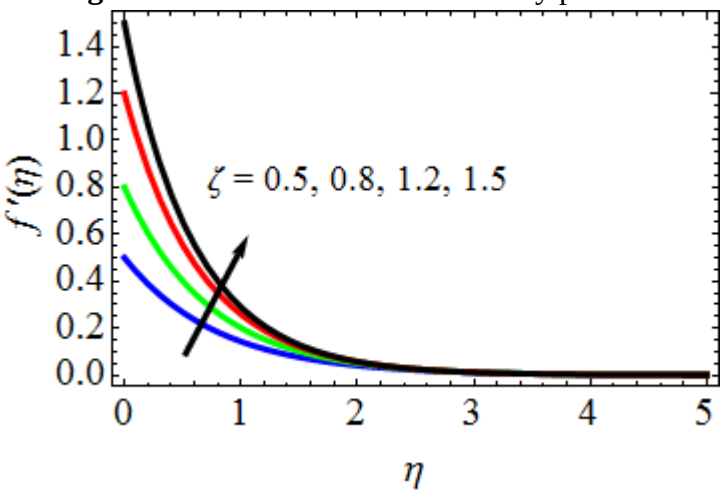

Fig. 7. Characteristics of ζ on velocity profiles

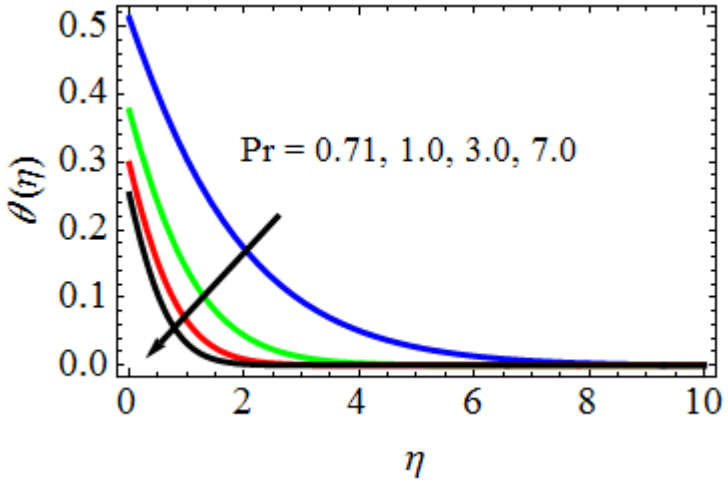

Fig. 8. Characteristics of Pr on temperature profiles

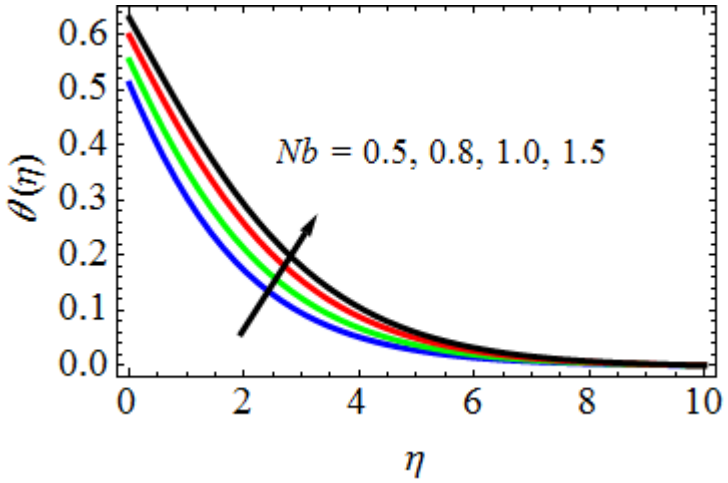

Fig. 9. Characteristics of *Nb* on temperature profiles

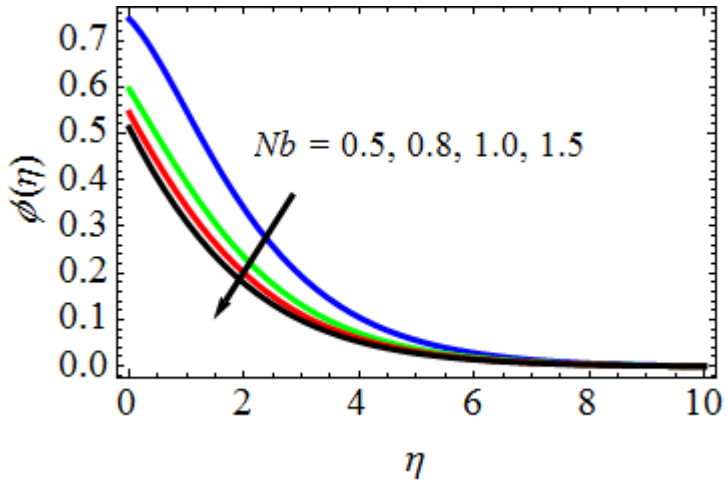

Fig. 10. Characteristics of *Nb* on concentration profiles

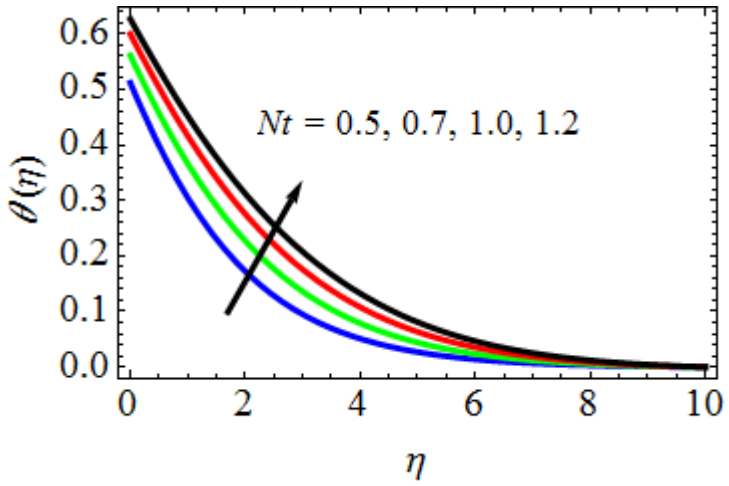

Fig. 11. Characteristics of *Nt* on temperature profiles

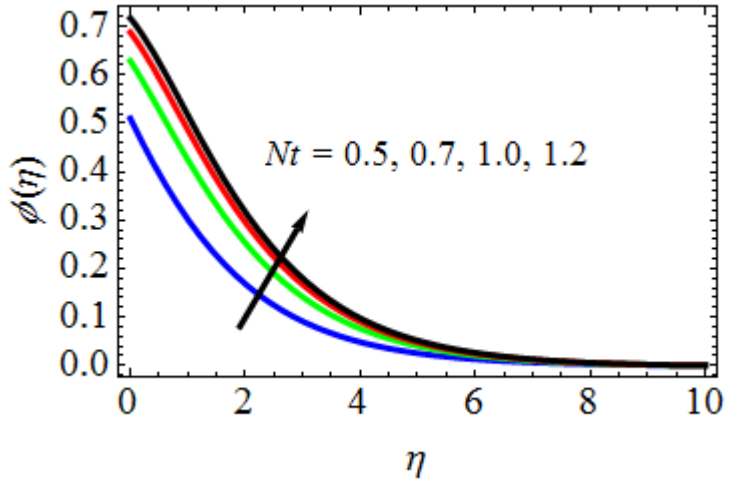

Fig. 12. Characteristics of *Nt* on concentration profiles

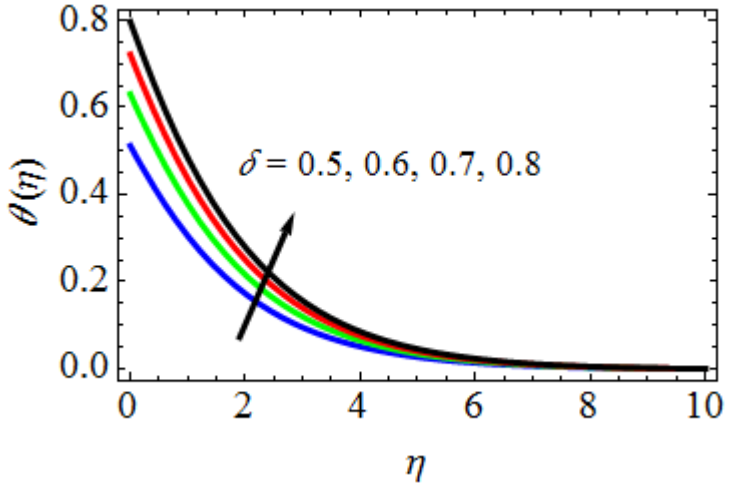

Fig. 13. Characteristics of δ on temperature profiles

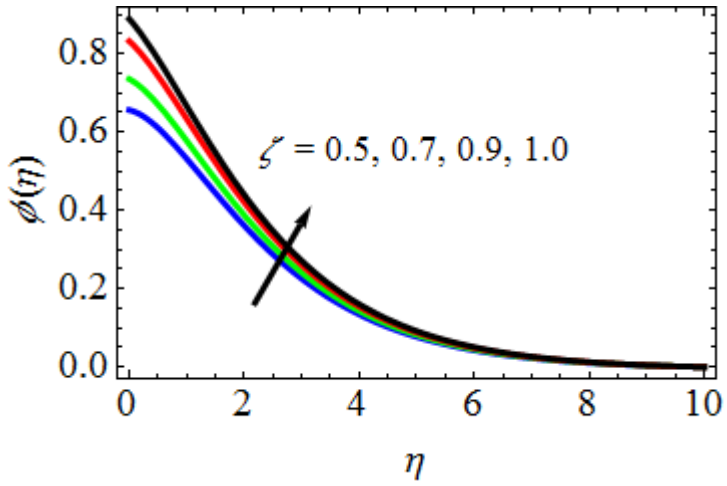

Fig. 14. Characteristics of ζ on concentration profiles

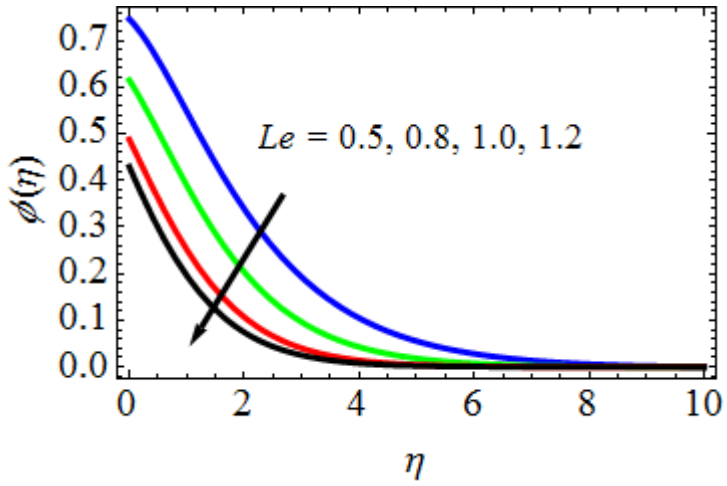

Fig. 15. Characteristics of *Le* on concentration profiles

Table-2.: Skin-friction coefficient results for variations of *M, K, λ, β, ϑ, S*, Pr, *Nt, Nb, δ, ζ* and *Le*

M	*K*	*λ*	*β*	*ϑ*	*S*	Pr	*Nt*	*Nb*	*δ*	*ζ*	*Le*	*Sh*
0.5	0.5	0.5	0.5	0.5	- 0.5	0.71	0.5	0.5	0.5	0.5	0.5	1.549413536546798
0.8												1.519834266714326
1.0												1.495682349805649
	0.7											1.521254387453246
	0.9											1.509806651236579
		0.6										1.560987932634687
		0.7										1.580098123414590
			0.8									1.556798223113484
			1.0									1.567738460876340
				0.7								1.567879564933857

				0.8								1.589318943986489
					- 0.1							1.517654876534063
					0.1							1.496781789743986
					0.5							1.470190384679139
						1.0						1.506871347830912
						7.0						1.480198698734698
							0.7					1.567681099068384
							1.0					1.583788198358925
								0.8				1.575398769384911
								1.0				1.590389698369819
									0.6			1.577859039814543
									0.7			1.586517634734732
										0.7		1.561643039403491
										0.9		1.570878738786396
											0.8	1.528734966756308
											1.0	1.508798304983301

The link among the Lewis number (Le), the Mass Biot number (), the Brownian motion component (Nb), & the thermophoresis parameter (Nt), referred to as the rate of transfer of mass or Sherwood number factor, is shown in Table 4. As observed in the table, the rate of mass transfer coefficient rises as the numbers of the Mass Biot number () and thermophoresis component (Nt) grow while decreasing as the values of the Lewis number (Le) and Brownian motion parameter (Nb) grow.

Table-3.: Nusselt number constant values for dissimilar standards of Pr, *δ*, *Nb* and *Nt*

Pr	*δ*	*Nb*	*Nt*	Nu_x
0.71	0.5	0.5	0.5	0.866783910763491
1.00				0.837887314987067
7.00				0.807438764307134
	0.6			0.886729871938367
	0.7			0.900988398398393
		0.8		0.896776304760347
		1.0		0.912456289458714
			0.7	0.891567034601373
			1.0	0.917847567103751

Table-4.: Sherwood number figure standards for dissimilar standards of *Le*, ζ, *Nb* & *Nt*

Le	*ζ*	*Nb*	*Nt*	Sh_x
0.5	0.5	0.5	0.5	1.104865365977898
0.8				1.056576513234387
1.0				1.011243564633568

	0.6			1.125673109876340
	0.7			1.147681783409619
		0.8		1.132657409734939
		1.0		1.151567943090343
			0.7	1.144671087650749
			1.0	1.156783198374562

6. Conclusions:

The current study examines the movement of an Eyring-Powell Nano fluid in the absence of a magnetic field, Brownian motion, thermophoresis, thermal, & mass Biot numbers along a stretched sheet plate held in a porous medium. The Runge-Kutta approximation approach and the shot method are used to solve the dimensionless calculations while the effects of the different physical factors are graphicall shown and discussed. Comparing well with analogous published efforts in the literature, the results in the limited scenario appear promising. The analysis reveals that:

- ✓ The rapidity profile reductions by growing levels of the magnetic arena limitation.
- ✓ The velocity ranges reduction as the permeability constant growths.
- ✓ The hotness and saturation fields are improved by increasing the thermophoresis variable.
- ✓ The temperature distribution is improved with a larger Brownian motion parameter.
- ✓ A rise in the thermal Biot number results in a decline in temperature fields.
- ✓ The flow and concentration characteristics improve as the mass Biot number rises.
- ✓ Greater Brownian motion Nb & Lewis amount Le values result in a lower concentration profile.
- ✓ Finally, for specific values of these variables, comparability of the current study work with that of Keller and Magyari [28] and El-Aziz [29] is taken into consideration.

References:

1. T. Hayat, S. Asghar, and M. Imtiaz. "MHD flow of Powell-Erying fluid over a permeable stretching sheet with thermal and mass Biot numbers." Journal of Molecular Liquids, vol. 202, pp. 253-258, 2015.
2. F. Ahmad, A. Alsaedi, and T. Hayat. "Stagnation point flow of Powell-Erying fluid with thermal and mass Biot numbers." Journal of the Brazilian Society of Mechanical Sciences and Engineering, vol. 40, no. 9, pp. 1-10, 2018.
3. A. Khan, M. Imtiaz, and T. Hayat. "MHD flow of Powell-Erying fluid with variable thermal and mass Biot numbers." Journal of Molecular Liquids, vol. 267, pp. 398-405, 2018.
4. M. Turkyilmazoglu and B. Tiryaki. "Heat and mass transfer in Powell-Erying fluid flow over a stretching sheet with variable thermal and mass Biot numbers." Journal of Molecular Liquids, vol. 284, pp. 282-292, 2019.
5. M. A. Rana, A. M. Siddiqui, and I. Khan. "Flow and heat transfer analysis of Powell-Erying fluid with thermal and mass Biot numbers." Alexandria Engineering Journal, vol. 60, no. 1, pp. 173-179, 2021.

6. Aziz, A., Abbas, Z., & Mustafa, M. (2016). Effects of thermal and mass Biot numbers on Powell-Erying fluid flow over a stretching surface. Journal of Molecular Liquids, 220, 1046-1052.
7. Sheikholeslami, M., & Ganji, D. D. (2017). Simulation of Powell-Erying fluid flow with thermal radiation and chemical reaction using Buongiorno's model. Journal of the Taiwan Institute of Chemical Engineers, 72, 142-153.
8. Hossain, M. A., & Khan, M. R. (2018). Numerical simulation of Powell-Erying fluid flow over a stretching sheet with thermal radiation and heat generation/absorption effects. Journal of Molecular Liquids, 249, 189-196.
9. Maiti, S., & Das, U. (2020). Effects of thermal and mass Biot numbers on Powell-Erying fluid flow and heat transfer over an unsteady stretching sheet. Journal of Thermal Analysis and Calorimetry, 139(3), 1923-1933.
10. Chamkha, A. J., & Ismail, A. I. M. (2021). Nonlinear radiative heat transfer and Biot numbers effects on Powell-Erying fluid flow over an inclined stretching sheet. Journal of the Brazilian Society of Mechanical Sciences and Engineering, 43(4), 174.
11. Jafari, M., Nazari, M., & Chamkha, A. J. (2019). Combined effects of thermal and mass Biot numbers on MHD Powell-Eyring fluid flow and heat transfer over a stretching sheet with convective boundary conditions. Journal of Molecular Liquids, 277, 1-10.
12. Malvandi, A., Bararnia, H., & Chamkha, A. J. (2018). Nonlinear convective heat and mass transfer in Powell-Eyring fluid over a stretching sheet with chemical reaction and thermal radiation. Journal of Molecular Liquids, 263, 134-144.
13. Chakraborty, S., & Das, S. (2017). Unsteady MHD Powell-Eyring fluid flow with heat and mass transfer over an oscillating vertical plate. Journal of the Brazilian Society of Mechanical Sciences and Engineering, 39(5), 1417-1432.
14. Ahmed, S., & Farooq, M. (2019). Numerical investigation of Powell-Eyring fluid flow over a nonlinear stretching sheet with thermal and mass Biot numbers. Journal of Thermal Analysis and Calorimetry, 135(1), 355-364.
15. Chamkha, A. J., & Issa, M. I. (2019). Effects of thermal and mass Biot numbers on magnetohydrodynamic Powell-Eyring fluid flow and heat transfer over a stretching sheet. International Journal of Heat and Mass Transfer, 139, 995-1005.
16. Abbasi, F. M., & Sheikholeslami, M. (2017). Mixed convection of nanofluid in a channel with variable thermal and mass Biot numbers. Journal of Molecular Liquids, 225, 716-725.
17. Abu-Nada, E., et al. (2020). Entropy generation in MHD mixed convection of a nanofluid in a lid-driven cavity with thermal and mass Biot numbers effects. International Journal of Heat and Mass Transfer, 160, 120218.
18. Afrand, M., et al. (2020). Numerical simulation of nanofluid flow over a stretching sheet with thermal and mass Biot numbers effects. International Journal of Heat and Mass Transfer, 161, 120228.
19. Chamkha, A. J., & Ismail, A. I. M. (2019). Effects of thermal and mass Biot numbers on magnetohydrodynamic Powell-Eyring fluid flow and heat transfer over a stretching sheet. International Journal of Heat and Mass Transfer, 139, 995-1005.

20. Chamkha, A. J., & Ismail, A. I. M. (2020). Magnetic field effects on nanofluid flow and heat transfer over an inclined stretching sheet with thermal radiation and mass Biot number. Journal of Molecular Liquids, 314, 113648.
21. Dehghan, M., et al. (2021). Nonlinear convection flow of a nanofluid considering the effects of thermal and mass Biot numbers. Journal of Thermal Analysis and Calorimetry, 145(1), 397-408.
22. Ghadikolaei, S. S., et al. (2018). Natural convection of water-Al2O3 nanofluid in a square cavity with localized heating from below: Buongiorno's mathematical model with Biot number effects. International Journal of Heat and Mass Transfer, 116, 1217-1227.
23. Ghasemi, B., & Aminossadati, S. M. (2018). Nanofluid flow and heat transfer over a stretching sheet with thermal and mass Biot numbers. Journal of Thermal Analysis and Calorimetry, 131(3), 2181-2191.
24. Hiremath, P. S., & Manjunatha, C. M. (2018). Combined effects of thermal radiation and chemical reaction on MHD free convective flow of a nanofluid with thermal and mass Biot numbers. Journal of Thermal Analysis and Calorimetry, 132(1), 371-384.
25. Reddy, M. G., & Kishan, N. (2017). Thermal radiation and mass transfer effects on MHD stagnation point flow of nanofluid with convective boundary condition. Journal of Molecular Liquids, 232, 342-350.
26. Rostamian, H., et al. (2021). Numerical analysis of MHD nanofluid flow and heat transfer considering thermal radiation and mass Biot numbers. Journal of Molecular Liquids, 327, 115188.
27. Turgut, A., & Karabay, H. (2016). Heat and mass transfer analysis of nanofluid flow with thermal and mass Biot numbers. International Journal of Heat and Mass Transfer, 93, 634-641.
28. E. Magyari and B. Keller, Heat and mass transfer in the boundary layers on an exponentially stretching continuous surface, J. Phys. D: Appl. Phys., 32, 577, (1999).
29. M. A. El-Aziz, Viscous dissipation effect on mixed convection flow of a Micropolar fluid over an exponentially stretching sheet, Can. J. Phys. 87, 359 (2009).